

Scanned-probe detection of electron spin resonance from a nitroxide spin probe

Eric W. Moore^{a,1}, SangGap Lee^{a,1}, Steven A. Hickman^a, Sarah J. Wright^a, Lee E. Harrell^b, Peter P. Borbat^a, Jack H. Freed^a, and John A. Marohn^{a,2}

^aDepartment of Chemistry and Chemical Biology, Cornell University, Ithaca, NY 14853-1301; and ^bDepartment of Physics, U.S. Military Academy, West Point, NY 10996

Edited by Adriaan Bax, National Institute of Diabetes and Digestive and Kidney Diseases, Bethesda, MD, and approved November 2, 2009 (received for review July 20, 2009)

We report an approach that extends the applicability of ultrasensitive force-gradient detection of magnetic resonance to samples with spin-lattice relaxation times (T_1) as short as a single cantilever period. To demonstrate the generality of the approach, which relies on detecting either cantilever frequency or phase, we used it to detect electron spin resonance from a $T_1 = 1$ ms nitroxide spin probe in a thin film at 4.2 K and 0.6 T. By using a custom-fabricated cantilever with a 4 μm -diameter nickel tip, we achieve a magnetic resonance sensitivity of 400 Bohr magnetons in a 1 Hz bandwidth. A theory is presented that quantitatively predicts both the line-shape and the magnitude of the observed cantilever frequency shift as a function of field and cantilever-sample separation. Good agreement was found between nitroxide T_1 's measured mechanically and inductively, indicating that the cantilever magnet is not an appreciable source of spin-lattice relaxation here. We suggest that the new approach has a number of advantages that make it well suited to push magnetic resonance detection and imaging of nitroxide spin labels in an individual macromolecule to single-spin sensitivity.

MRFM | ESR | TEMPAMINE | mechanically detected magnetic resonance | molecular structure imaging

A generally applicable approach for determining the tertiary structure of an individual macromolecule in vitro at angstrom or subangstrom resolution would create exciting opportunities for answering many longstanding questions in molecular biology. For macromolecules too large to characterize by NMR or X-ray diffraction, the tertiary structure of proteins (1–3), nucleic acids (4, 5), and biomolecular assemblies (6, 7) can be explored by using inductively-detected electron spin resonance (ESR) to measure distances between pairs of attached spin labels (2–5, 7, 8). These studies, however, require bulk quantities of sample (9) and demand multiple experiments with spin labels attached to different locations in the target macromolecule. Mechanical detection and imaging of single-electron spins has been demonstrated, in E' centers in gamma-irradiated quartz (10), and it is natural to explore applying magnetic resonance force microscopy (MRFM) (11–15) to map the locations of individual spin labels attached to a single biomacromolecule.

The ultimate limit of imaging resolution in MRFM is set by the intrinsic linewidth of the resonance and the applied magnetic field gradient. For a 0.1 mT homogeneous linewidth, typical of the organic radical studied here, a gradient of 4×10^6 T/m allows selective excitation of individual spin labels only 0.025 nm apart. A magnetic field gradient this large has recently been demonstrated in an MRFM experiment by using ferromagnetic pillars fabricated by electron-beam lithography (15). The force sensitivity required to detect single electrons in this gradient is 40 aN, above the minimum detectable force (in 1 Hz bandwidth) of 5 – 10 aN reported for a high-compliance cantilever operated with its metalized leading edge above a metal-coated surface in high vacuum at 300 mK (15). In all high-sensitivity MRFM experiments to date, sensitivity has been limited by interactions of the cantilever with fluctuating electric fields and electric field gradients originating in

the sample substrate. Efforts to mitigate this surface noise via careful sample preparation and by fabricating magnetic tips that extend beyond the leading edge of the cantilever are progressing rapidly.

Before these improvements in sensitivity and resolution can be harnessed to study organic spin labels, a suitable method must be devised for creating a distinguishable spin signal. Unfortunately, organic spin labels do not meet the stringent sample requirements of established mechanical single-spin detection protocols (10). The force-based interrupted oscillating cantilever adiabatic reversals (i-OSCAR) approach, used by Rugar et al. to detect single-electron spins in quartz (10), requires samples with rotating-frame spin-lattice relaxation times of $T_{1\rho} \geq 0.1$ s to reach single-spin sensitivity. At low temperatures, we expect nitroxide spin labels to have spin-lattice relaxation times in the range $1 \text{ s} \geq T_1 \geq 1 \text{ ms}$ and $T_{1\rho}$'s of only a few μs (16–18), making signal modulation by i-OSCAR (19) inapplicable. Cyclic adiabatic inversion (15) is likewise inapplicable because it relies on continuous spin locking. Saturating the sample spins cyclically is another approach to creating a distinguishable signal (20, 21). To achieve high sensitivity, spin magnetization should be modulated at the cantilever's resonance frequency. Cyclic saturation thus requires samples with spin-lattice relaxation times less than the cantilever period, $T_1 < T_c$, which would necessitate using cantilevers with impractically low resonance frequencies, given the expected range of T_1 for nitroxides at low temperatures. The force-gradient approach to mechanically detecting spins introduced by Garner et al. (13) can in principle be used to create a detectable spin signal from a nitroxide spin label. In practice, however, cantilever-enabled readout of magnetization inversion transients (CERMIT) has to date (13, 22) only been used to observe magnetic resonance from spins with $T_1 \gg 0.1$ s and, moreover, has relied on adiabatic rapid passage to flip spins and create a distinguishable signal.

Here we introduce an improved force-gradient approach to mechanically detecting magnetic resonance that is applicable to samples — such as nitroxide spin probes — with T_1 's as short as ≈ 0.2 ms. We demonstrate the approach by using a magnetic-tipped ultrasensitive cantilever operated at high magnetic field to detect ESR from a thin-film containing the nitroxide spin probe 4-amino-2,2,6,6-tetramethylpiperidine-1-oxyl (TEMPAMINE) widely used in ESR studies of biomolecules. The expanded force-gradient approach to mechanical detection of magnetic resonance introduced here requires only milligauss microwave magnetic fields to detect ESR from a nitroxide free radical, is well suited to the study of thin-film samples, and

Author contributions: E.W.M., S.L., J.H.F., and J.A.M. designed research; E.W.M., S.L., S.A.H., S.J.W., L.E.H., and P.P.B. performed research; S.L., S.A.H., S.J.W., and L.E.H. contributed new reagents/analytic tools; E.W.M. and S.J.W. analyzed data; and J.A.M. wrote the paper.

The authors declare no conflict of interest.

This article is a PNAS Direct Submission.

¹E.W.M. and S.L. contributed equally to this work.

²To whom correspondence should be addressed. E-mail: jam99@cornell.edu.

This article contains supporting information online at www.pnas.org/cgi/content/full/0908120106/DCSupplemental.

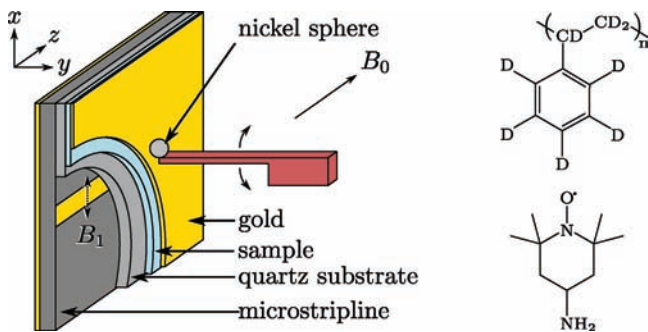


Fig. 1. Scanned-probe ESR experiment schematic. A microstripline half-wave resonator delivers a transverse magnetic field, B_1 , oscillating at 17.7 GHz. In the center of the resonator, the microwave field oscillates along the x direction. A longitudinal Zeeman field of magnitude $B_0 \approx 0.6$ T is applied along the z axis. The high-compliance cantilever has its long axis along y and oscillates in the x direction. The cantilever's $4 \mu\text{m}$ -diameter nickel tip was affixed by hand. The sample is a 230 nm -thick film of 40 mM TEMPAMINE in perdeuterated polystyrene, coated with 20 nm of gold. The sample film was spin-coated onto a $250 \mu\text{m}$ -thick quartz wafer. For clarity, sample and substrate are not drawn to scale.

is compatible with magnetic-tipped attonewton-sensitivity cantilevers at high magnetic field. The new method is capable of detecting magnetic resonance in samples whose spin-lattice relaxation times are as short as a single cantilever period, extending the lower limit of sample relaxation times that can be detected by using force-gradient methods by $\geq 10^2$. Our findings moreover show that saturation, when married to force-gradient detection, can be used to create a detectable signal even when $T_1 \gg T_c$. This combination of capabilities opens up new avenues for pushing detection and imaging of ESR from a wide range samples, particularly nitroxide spin probes, toward single-spin sensitivity.

Results

Experiments were carried out in high vacuum at liquid helium temperatures. The central component of the experiment is a high-compliance cantilever (23, 24) with spring constant $k_0 = 7.8 \times 10^{-4} \text{ N/m}$, resonance frequency $f_0 = 4,975 \text{ Hz}$, mechanical quality factor of $Q = 1.05 \times 10^5$, and force sensitivity of $F_{\text{min}} = 7.5 \times 10^{-18} \text{ N}$ in a 1 Hz bandwidth at a temperature of $T = 4.2 \text{ K}$ and in a vacuum of $P = 10^{-6} \text{ mbar}$. A nickel sphere of diameter $4 \mu\text{m}$ was affixed to the end of the cantilever manually and held in place with epoxy. See Fig. 1 for a sketch of the experiment and sample details.

The sample was prepared by spin casting TEMPAMINE and perdeuterated polystyrene onto a quartz substrate and coating the resulting film with a thin layer of gold (see *SI Appendix* for details). A small voltage was applied between the cantilever and the gold coating to minimize noncontact friction (25–27) and surface frequency noise (10, 28). In parallel, samples were prepared in the same way (minus the gold layer), manually removed from the substrate, and inserted into a quartz tube for characterization by inductively detected pulsed ESR at low temperatures.

The cantilever was brought over the thin-film sample, located in the x - z plane of Fig. 1, with the long axis of the cantilever along the y axis such that the cantilever oscillated in the x direction. A static magnetic field was applied along the z direction, parallel to the width of the cantilever (13, 29). We applied the field along the width of the cantilever in order to mitigate damping of the cantilever arising from tip-field interactions (30). A microstripline half-wave resonator delivered a microwave magnetic field oscillating in the x direction. The cantilever was excited into self-oscillation via a piezo mounted at the cantilever base by using a fixed-gain positive feedback loop (31). Cantilever position was detected by using a fiberoptic interferometer ($\lambda = 1,310 \text{ nm}$,

incident power $3 \mu\text{W}$), digitized, and sent to a high-bandwidth software frequency demodulation algorithm (28).

We detect small shifts in the cantilever frequency due to spring constant changes arising from spin-tip interactions. In the experimental geometry of Fig. 1, sample spins interact with the magnetic tip of the cantilever to shift the mechanical spring constant of the cantilever by an amount

$$\Delta k_m = \sum_j \mu_{z,j} \frac{\partial^2 B_z^{\text{tip}}}{\partial x^2}, \quad [1]$$

where $\mu_{z,j}$ is the z -component of the magnetic moment of the j th spin in the sample and $G' \equiv \partial^2 B_z^{\text{tip}} / \partial x^2$ is the second derivative of the tip field's z component, B_z^{tip} , with respect to the oscillation direction x . The sum is over all spins in the sample. To create a distinguishable signal, we flip spins in a region below the tip via magnetic resonance. To achieve these spin flips, we turn on the microwave field, in synchrony with the cantilever oscillation, for a half-cantilever period every few periods (Fig. 2). Spins at a certain distance from the tip are partially saturated and this “saturated slice” is swept through the sample to create a region of diminished electron spin magnetization. The location of the saturated slice is determined by the microwave frequency, the tip magnetization, the tip-sample separation, and the static field. The microwave field is turned off for $n - 1/2$ cycles, during which time the saturated-slice magnetic moment μ^{res} recovers towards equilibrium. During these n cycles the cantilever receives a phase kick of

$$\Delta \phi \approx \frac{\pi f_0}{k_0} \mu_z^{\text{res}} G' \int_0^{nT_c} e^{-t/T_1} dt = \frac{\pi f_0 \mu_z^{\text{res}} G' T_1}{k_0} (1 - e^{-nT_c/T_1}), \quad [2]$$

where T_c is the cantilever period, T_1 is spin-lattice relaxation time (assumed to be the same in each saturated slice), and where we assume that $\Delta k_m \ll k_0$ (valid here). After n cycles, the microwave field is reapplied and the slice's spin magnetization resaturated. As a result of the repeated saturation, the cantilever's frequency change is approximately

$$\Delta f_c \approx \frac{1}{2\pi} \frac{\Delta \phi}{nT_c} \approx \frac{f_0}{2k_0} \times \mu_z^{\text{res}} G' \quad [3]$$

when $nT_c \ll T_1$, which will be approximately the case here.

To more easily detect this tiny frequency shift, the shift is modulated at frequency $f_{\text{mod}} \approx 6.48 \text{ Hz}$. This modulation is achieved by turning on and off the microwave field every $\approx 1/2f_{\text{mod}}$ seconds, again in synchrony with the cantilever oscillation. The cantilever frequency from the demodulator is sent to a software lock-in amplifier operating at reference frequency f_{mod} . The modulation is a square wave of amplitude Δf_c , resulting in a lock-in output whose primary frequency component has a root-mean-square amplitude of $\delta f_c = \sqrt{2} \Delta f_c / \pi$.

A plot of δf_c versus longitudinal field B_0 is shown in Fig. 3 for various tip-sample separations. The peak at field B_b occurs near the Larmor frequency of $B^{\text{res}} = f_{\text{mw}}/\gamma_e = 0.63 \text{ T}$ and its location is independent of tip-sample separation; this peak we assign to a “bulk” resonance in which the tip magnet is coupled to a large number of spins far away from the tip. The signal peak at field B_c is from spins seeing a tip-field opposing the longitudinal field. Assuming a tip magnetization of $\mu_0 M_{\text{tip}} = 0.6 \text{ T}$ as expected for nickel, a tip field of approximately $-\mu_0 M_{\text{tip}}/3 = -0.2 \text{ T}$ is expected for spins directly below a spherical tip at small tip-sample separation. These spins require a longitudinal field of $B^{\text{res}} + 0.2 \text{ T} \approx 0.8 \text{ T}$ to achieve resonance, in rough agreement with field value B_c . We assign the peak at field B_c as due to a “local” signal — a relatively small number of spins in resonance directly below the tip. The location of the signal peak at field B_d and the change of signal sign between field B_b and B_c can only be understood by simulating the

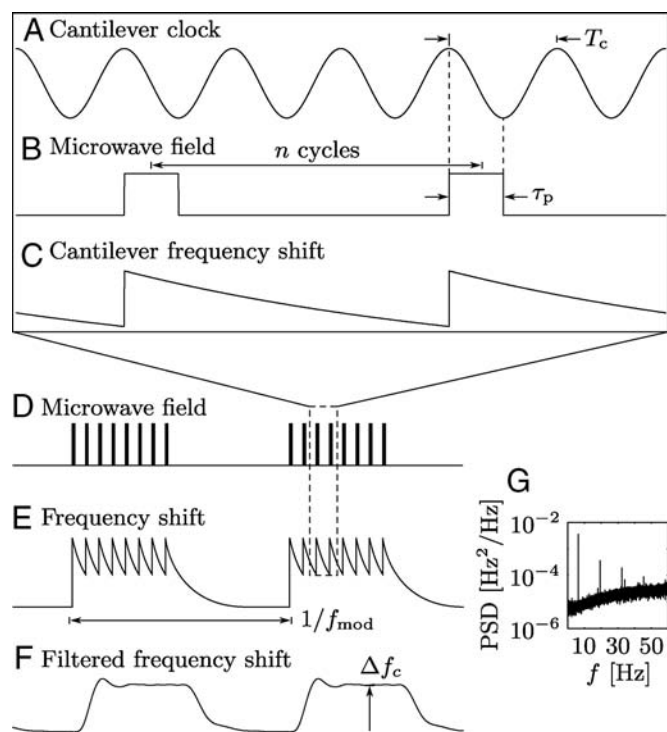


Fig. 2. Protocol for force-gradient detection of $T_1 \sim 1$ ms spins. (A) The cantilever is self-oscillated at its mechanical resonance frequency (4,975 Hz; cantilever period $T_c = 201 \mu\text{s}$) to an amplitude of $x_{\text{rms}} = 233$ nm. (B) When the cantilever is at its maximum positive displacement, a microwave switch is turned on. The applied microwave field (partially) saturates the sample's electron spins, which relax over a few cantilever cycles. The microwave field remains on for a half of a cantilever period, $\tau_p = T_c/2 \approx 100.5 \mu\text{s}$, during which time a region or "slice" of partially saturated spin magnetization is swept out in the sample. (A series of short pulses are used to minimize sample heating; a single long pulse would also be effective.) (C) This sample magnetization interacting with the second derivative of the cantilever's tip field shifts the mechanical frequency of the cantilever. The microwave field is reapplied, in synchrony with the cantilever oscillation, every few (n) cycles. (D) This procedure is repeated for approximately 77 ms, followed by a 77-ms period, during which no microwave field is applied. (E and F) The resulting modulation of the cantilever frequency contains components at the pulse frequency (E); however, we are sensitive only to the slower modulation (F) within the demodulation bandwidth ~ 60 Hz. The on-off cycling of the microwave pulses introduces a modulation of the cantilever frequency at f_{mod} . (G) The cantilever frequency power spectral density versus frequency under the scheme of A–F. The largest peak is at $f_{\text{mod}} = 6.48$ Hz. The modulation is well approximated by a square wave, and higher odd harmonics of f_{mod} are also visible.

spins in resonance at a given field and by considering the sign of G' experienced by each spin in-resonance. This analysis requires detailed numerical simulations to be described below.

A worry with detecting magnetic resonance mechanically, particularly of electron spins, is that spin diffusion (32) or thermomagnetic fluctuations in the tip (33–35) might deleteriously lower the sample's relaxation time. To address these concerns, we measured T_1 both mechanically and by pulsed ESR at the same temperature and field. We also measured T_2 by pulsed ESR by using electron spin echos (see the *SI Appendix* for details).

Although we can in principle measure T_1 from a plot of frequency shift δf_c versus pulse delay n (Eqs. 2 and 3; Fig. 2), we found that a small but present microwave-induced background change in the cantilever frequency made this approach highly problematic (see *SI Appendix*). We therefore developed an alternative phase-based protocol (Fig. 4) for measuring T_1 that yielded much cleaner data. Here, as in Fig. 2, the microwave field was applied for half of a cantilever cycle to create a region of diminished spin magnetization below the tip. The sample magnetization

recovers for $n = 1 - 32$ cycles, during which time the cantilever phase is advanced because of interactions with sample spins by $\Delta\phi$ (Eq. 2). Thirty-two microwave pulses are applied, and the net phase shift, $\Delta\phi^{\text{tot}} = 32\Delta\phi$, is inferred by comparing the phase before and after the period of microwave irradiation. We limited the number of repetitions to 32 so that the longest irradiation period, $32 \times 32 \times T_c \approx 0.2$ s, was much shorter than the cantilever phase memory time (e.g., ringdown time) of ≈ 5 s.

The resulting $\Delta\phi^{\text{tot}}$ versus n data are remarkably well described by Eq. 2 (Fig. 5). Fitting the data quantitatively required adding a small n -independent term to Eq. 2 to account for two expected effects: background microwave-induced phase kicks plus a phase advance arising from spin interactions with the cantilever during the half cycle of interaction present even when $n = 1$. The fits are excellent, and the T_1 measured for both bulk and local peaks are identical. Moreover, the T_1 's measured mechanically agree very well with $T_1 = 1$ ms measured by inductively detected pulsed ESR.

The finding that $T_1 \approx 1$ ms validates the assumption implicit in Eq. 1 that T_1 is longer than the cantilever period of $T_c = 0.2$ ms. In order to proceed with numerically simulating the signal of Fig. 3, we verified that we were changing sample magnetization by saturation and not, for example, by adiabatic inversion (19, 34). In Fig. 6, we plot the spin signal δf_c versus microwave power P delivered to the stripline resonator. We can see that both the local- and

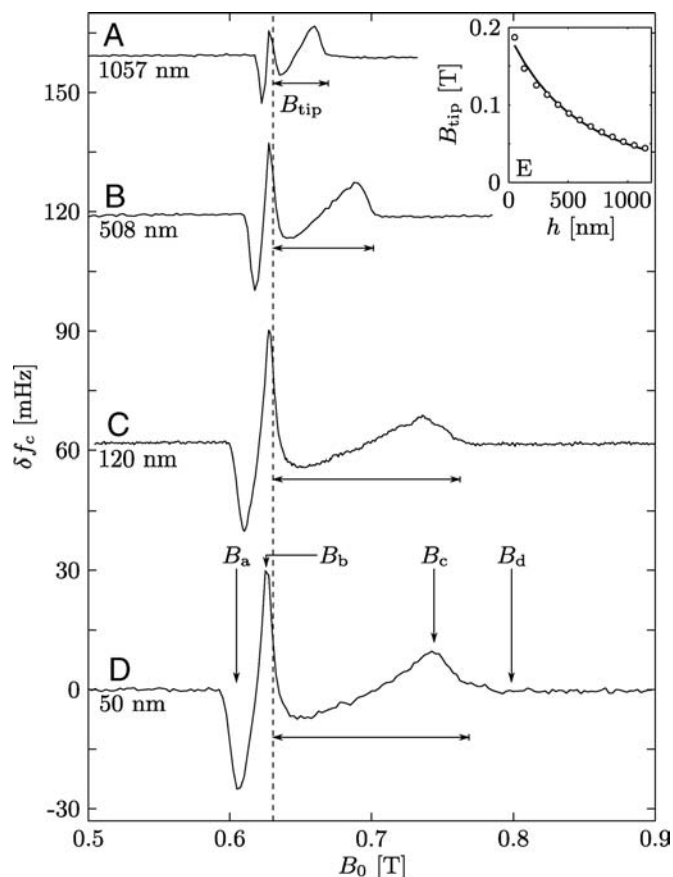


Fig. 3. Force-gradient detected ESR from TEMPAMINE, acquired by using the protocol of Fig. 2 with $n = 3$. (A–D) Fourier component of the cantilever frequency at $f_{\text{mod}} = 6.48$ Hz versus longitudinal field. The signal was acquired with detection bandwidth $b = 0.45$ Hz and microwave frequency $f_{\text{mw}} = 17.7$ GHz. The signal was averaged for 10 s/pt with a field step of 2.5 mT between each point for (A, B, and D) and 0.5 mT for C. (E) The tip field B_{tip} (indicated with arrows) was estimated as the separation between $B^{\text{res}} = 0.63$ T and the high-field edge of the signal and plotted versus tip-sample separation h . The data was fit to Eq. 4 to give a tip radius of $r_{\text{tip}} = 1.85 \pm 0.05 \mu\text{m}$ and a tip magnetization of $\mu_0 M_{\text{tip}} = 0.44 \pm 0.1$ T.

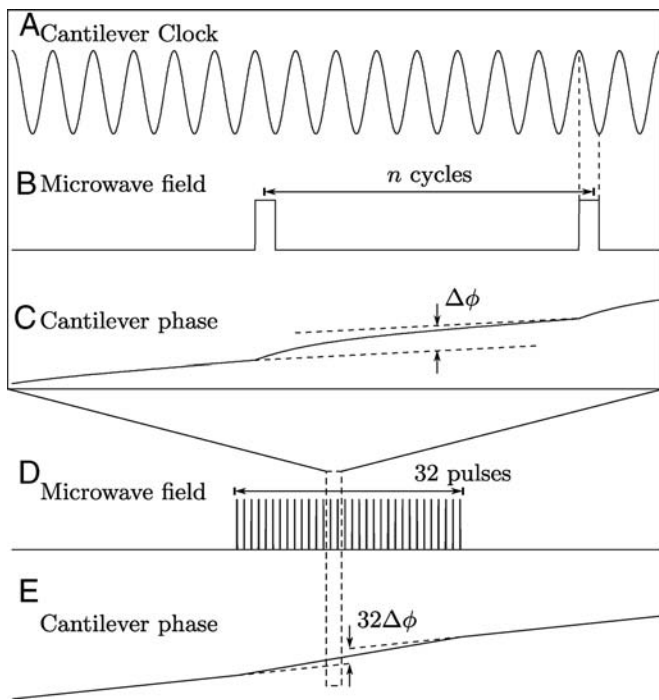


Fig. 4. Modified force-gradient protocol for measuring the sample spin-lattice relaxation time of $T_1 \sim 1$ ms spins via observation of cantilever phase shift. (A) As in Fig. 2, the cantilever is self oscillated and the microwave field (B) is turned on for a half cantilever cycle every n cycles to saturate the sample spins. To measure the spin-lattice relaxation time the delay n is stepped from 1 to 32 cycles. The spin-induced cantilever frequency shift leads to a phase shift (C), $\Delta\phi(n)$, which depends on the ratio of the repetition time nT_c to the spin relaxation time T_1 . (D) A total of 32 pulses are applied, resulting in a net cantilever phase shift (E) of $32\Delta\phi(n)$. The cantilever phase is measured for a time $T_{\Delta\phi}^{\text{acq}} = 0.41$ s, before and after application of the microwave field. The irradiation period was 0.2 s. The two phase-versus-time signals are fit to a line and the spin-induced phase shift computed by comparing the before and after intercepts.

bulk-peak signals saturate above $P \approx 100$ mW. Modeling the spin magnetization by using Bloch equations, we fit the data of Fig. 6 to $\delta f_c = \delta f_c^{\text{pk}} S / (1 + S)$ with δf_c^{pk} the peak frequency shift and $S = Pc_p^2 \gamma_e^2 T_1 T_2$ the saturation factor. Here c_p is a “coil constant” relating the power delivered to the stripline resonator and the

magnitude B_1 of the resulting transverse magnetic field; as defined, $B_1^2 = c_p^2 P$. Taking $T_2 = 450$ ns from inductively detected pulsed ESR measurements, we infer a coil constant of $c_p = 14$ mG/ $\sqrt{\text{W}}$. At a given applied power, we can now determine the saturation factor S from Fig. 6 or, alternatively, from c_p , T_1 , and T_2 .

To numerically simulate the signal, it remains to model the field and the field second derivative from the tip. We estimated the tip diameter and magnetization by studying the signal (δf_c versus B_0) as a function of the tip-sample separation h (Fig. 3). At each h , the tip field B_{tip} was estimated from the signal as the difference between the resonance field $B^{\text{res}} = f_{\text{rf}}/\gamma_e = 0.6305$ T and the high-field edge of the local peak. A plot of B_{tip} versus h can be seen in the inset of Fig. 3. The tip was modeled as a uniformly magnetized sphere and the data of Fig. 3E fit to

$$|B_{\text{tip}}| = \frac{\mu_0 M_{\text{tip}}}{3} \left(\frac{r_{\text{tip}}}{r_{\text{tip}} + h} \right)^3, \quad [4]$$

with $\mu_0 M_{\text{tip}}$ the tip magnetization and r_{tip} the tip radius. The observed B_{tip} versus h is well described by Eq. 4 with $\mu_0 M_{\text{tip}} = 0.44 \pm 0.1$ T, in reasonable agreement with $\mu_0 M_{\text{sat}} = 0.6$ T expected for the saturation magnetization of nickel. The inferred tip radius $r_{\text{tip}} = 1.85 \pm 0.05$ μm , is in excellent agreement with 2.0 ± 0.1 μm , estimated from a scanning electron micrograph of the tip (see *SI Appendix*).

Finally, the signal of Fig. 3 was numerically simulated by modeling the tip as a uniformly magnetized sphere, approximating the sample as a finite box, calculating B and G' at each location in the sample box and summing the contribution to Eq. 1 from all spins in resonance. As in the experiment, the local field was swept by translating the cantilever. Bloch equations were used to calculate μ_z by using the measured S , neglecting decay of magnetization during the cantilever cycle. Sample magnetization was calculated from the known concentration of TEMPAMINE and the Curie law.

The numerical simulation (Fig. 7) agrees remarkably well with the observed signal, assuming a sample temperature of $T = 11$ K. The simulation properly predicts not only the multiple sign changes in the observed frequency shift as the field is increased but also the correct absolute size of the observed frequency shift. Plotting the spins in resonance at selected fields confirms our assignment of the signal at field B_d as due to spins directly below the tip and helps us understand a number of initially puzzling features of the signal. For example, we can see that the signal goes

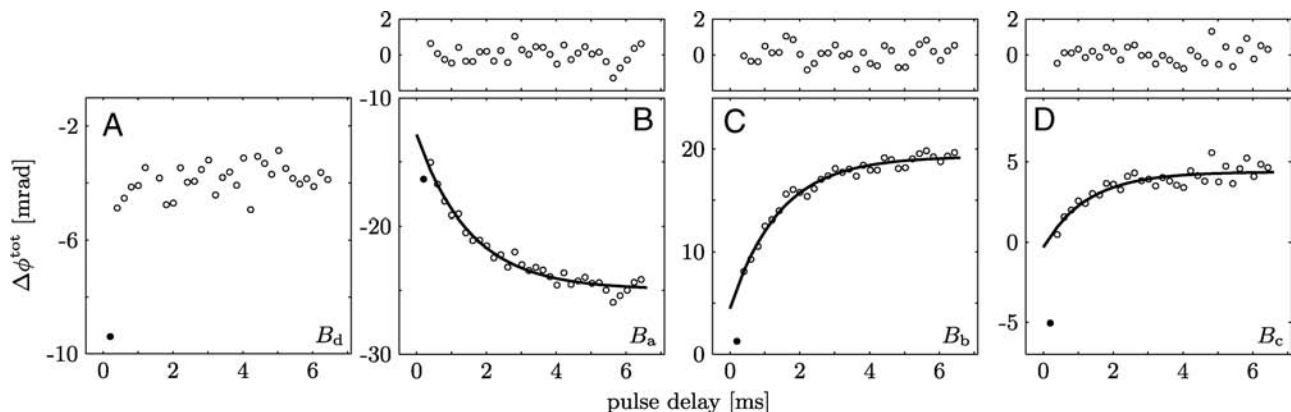


Fig. 5. Phase-based measurement of sample spin-lattice relaxation time. (A–D) Cantilever phase shift versus delay time at a field $B_d = 0.8000$ T at which no spins are in resonance (A) and at fields B_a , B_b , and B_c (B–D) (Fig. 3). The phase shift data (open circles) were fit to $\Delta\phi^{\text{tot}} = \Delta\phi^{\text{pk}}(1 - e^{-\tau_d/T_1}) + \Delta\phi^{\text{backnd}}$ (solid line) with $\tau_d = nT_c$ the pulse delay, $\Delta\phi^{\text{pk}}$ the peak phase shift, T_1 the spin-lattice relaxation time, and $\Delta\phi^{\text{backnd}}$ a background phase kick (see *Results* for details). The phase shift at the $n = 1$ delay was anomalous (filled circles) and excluded from the fits. Fit residuals are displayed on top. The measured spin-lattice relaxation times are $T_1 = 1.41 \pm 0.24$ ms at $B_a = 0.6125$ T, $T_1 = 1.53 \pm 0.29$ ms at $B_b = 0.6275$ T, and $T_1 = 1.27 \pm 0.63$ ms at $B_c = 0.7200$ T. Each point is the average of 25 runs of $T_{\Delta\phi}^{\text{acq}} = 0.41$ s each.

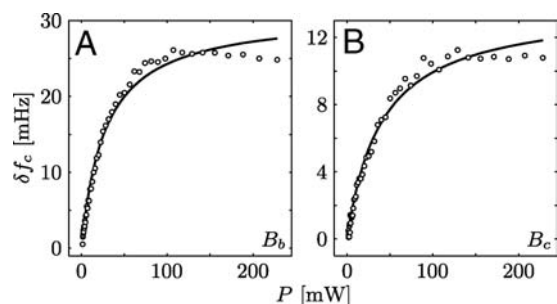


Fig. 6. The dependence of ESR signal on microwave power for the (A) “bulk” peak at field $B_b = 0.6275\text{ T}$ and (B) “local” peak at $B_c = 0.7200\text{ T}$. The data was fit to $\delta f_c = \delta f_c^{pk} S / (1 + S)$ with δf_c^{pk} the peak frequency shift and $S = P c_p^2 \gamma_e^2 T_1 T_2$ the saturation factor, with $T_1 = 1.3\text{ ms}$ and $T_2 = 450\text{ ns}$ to give a coil constant of $c_p = 14\text{ mG}/\sqrt{\text{W}}$.

to zero between fields B_b and B_c because of a cancellation of net G' , which can be both positive and negative, when summed over the spins in resonance. We can also see that the signal peak at B_a is indeed due to spins far away from the tip which experience a positive G' and, unlike most spins contributing to the signal, a positive field from the tip.

Discussion

Sensitivity. To estimate the spin sensitivity of our experiment, we convert the measured frequency noise to an equivalent spring-constant noise and then use Eq. 1 to calculate an equivalent magnetic moment noise. The result is $P_\mu = 4k_0^2 P_{sf} / f_0^2 G'^2$. The measured frequency noise at height $h = 120\text{ nm}$, drive amplitude $x_{rms} = 233\text{ nm}$, and frequency offset $f_{mod} = 6.48\text{ Hz}$ is approximately $P_{sf} = 1 \times 10^{-6}\text{ Hz}^2/\text{Hz}$ (see *SI Appendix*), 100 times the noise expected from thermomechanical cantilever motion (28, 31). Spins directly below the tip — those giving rise to the signal at field B_c in Fig. 3 — experience the largest G' and therefore couple most strongly to the tip. From the simulations of Fig. 7, we infer that G' varies from $-1 \times 10^{10}\text{ T/m}^2$ to $8.5 \times 10^{10}\text{ T/m}^2$ for the spins in this slice. Taking the larger of these two values gives a minimum detectable magnetic moment of $\mu_{min} = (P_\mu b)^{1/2} = 4 \times 10^2\ \mu_B$ in a $b = 1\text{ Hz}$ bandwidth.

This sensitivity is comparable with the $184\ \mu_B\text{ Hz}$ sensitivity (in 1 Hz bandwidth) achieved by Bruland et al. (36) who used a magnetic tip similar in diameter to ours, a soft commercial Si_3N_4 cantilever, and cyclic saturation to detect ESR from DPPH at 77 K. Kuehn et al. (14) have shown that force detection (via i-OSCAR) has equivalent signal to noise to force-gradient detection when the tip is adjusted to have amplitude $x_{0p}^c = 0.47 (r_{tip} + h)$. Here $x_{0p}^c = 330\text{ nm}$ to avoid saturating the interferometer. Setting h to $1\ \mu\text{m}$ to reduce surface noise and using $x_{0p}^c = 1.5\ \mu\text{m}$ to maximize the sensitivity would improve μ_{min} to $1 \times 10^2\ \mu_B$, comparable with that achieved in ref. 36. The detection approach demonstrated here is a significant advance over the Bruland et al. experiment because it is compatible with high-sensitivity cantilevers oscillating parallel to the surface and works for samples with $T_1 \geq 0.2\text{ ms}$, such as nitroxides.

Single-Electron Sensitivity. Even with a carefully-chosen sample and meticulously designed cantilever (37), magnetic tip (33–35), microwave source (38), and protocols to detect spin fluctuations (19), 12 hr of signal averaging per point was required to observe single-electron spins via i-OSCAR detection in the experiment of ref. 10. To image individual nitroxide spin labels in a reasonable time, detection of individual electrons must be accomplished in a few seconds or minutes. Our findings suggest two modifications that will enable rapid detection of individual electron spins, which are described as follows.

Boltzmann polarization and signal averaging. The Curie-law spin polarization is $p = 0.037$ here. Decreasing temperature to 300 mK and increasing operating frequency to 50 GHz gives $p = 0.999$. Having such a fully polarized spin as the initial condition dramatically improves the efficacy of signal averaging because the improvement in the power signal-to-noise ratio with the number of averages N scales as $\propto N$ for Curie-law signal, in comparison with the $\propto N^{1/2}$ scaling for a stochastic spin-fluctuation signal (10).

Spin modulation. The protocol of Fig. 2 is suitable for a single-spin experiment. With the microwaves on, spin nutation randomizes the magnetic moment of a single spin to zero over the time of a cantilever cycle. The randomly oriented spin takes a time T_1 , on average, to realign with the field via spin-lattice relaxation. The interaction of the single spin with the cantilever will thus, on average, reproduce the ensemble-average behavior depicted in Fig. 2. The modulation frequency in Fig. 2 need only satisfy $f_{mod} \ll 1/T_1$, and one is at liberty to set f_{mod} to avoid surface noise (at low f) and detector noise (at high f).

Modifying the magnet-on-cantilever apparatus of ref. 10 by replacing the irradiated quartz sample with a thin-film, nitroxide-labeled biopolymer sample, working at higher field and lower temperature, and by using the Fig. 2 protocol to detect Curie-law polarization instead of the i-OSCAR protocol to detect stochastic polarization, we estimate that achieving a power signal-to-noise of 4 would require only 3.5 min of signal averaging. This acquisition time and SNR is already sufficient to collect a 1.2×10^3 pixel image in three days. If we are willing to place the nitroxide-labeled biopolymer sample on the cantilever, we can outfit the apparatus of ref. 15 with a microwave microwire. Although the frequency noise in the ref. 15 is unknown, if we assume that it is limited by cantilever thermomechanical fluctuations, the minimum detectable magnetic moment (in a 1 Hz bandwidth) is $0.27\ \mu_B$, which would enable the acquisition of a 64^3 -pixel image in three days.

Our approach to mechanically detecting ESR has substantially fewer technical constraints than the approach of ref. 10.

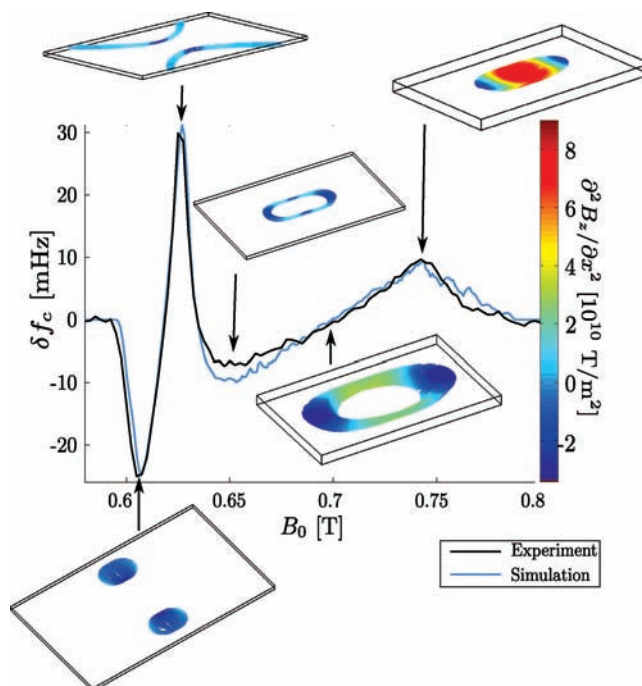


Fig. 7. Simulation of the frequency shift, δf_c , versus magnetic field for a tip-sample height of 50 nm. The sensitive slice is shown for a selection of field values, colored by the second derivative of the tip field. The simulation is fit to the Fig. 3D data by using only sample temperature as a free parameter.

These relaxed requirements give us significant leeway to improve per-spin sensitivity.

Microwave source. We used a microwave field of rotating-frame amplitude $B_1 = 3.9$ mG to saturate spins and create a distinguishable signal whereas a $B_1 = 3$ G field and adiabatic inversion was used in ref. 10. Although saturation gives a signal half as large as adiabatic inversion, it requires (with a better optimized resonator than ours) (see *SI Appendix*) only 10^{-3} times the microwave field and 10^{-6} times the microwave power — a significant advantage because microwave heating of the cantilever is a concern at low temperature (10, 38). The smaller required B_1 gives us the freedom to employ a nonsuperconducting resonator and metal coat the sample to reduce surface noise.

Cantilever design. Thermal motions of the cantilever tip create a fluctuating magnetic field that, if the motions have spectral density near the Rabi frequency, can be a potent source of $T_{1\rho}$ relaxation (37). To obtain long signal coherence times in i-OSCAR experiments, it was necessary to fabricate complex hinged cantilevers with suppressed higher-megahertz-frequency modes (10). In contrast, the signal coherence time in our experiment is set by T_1 and therefore sensitive only to cantilever motions at the Larmor frequency of 17 GHz, which are negligible for an audio-frequency cantilever. Thus, a simple beam cantilever should be sufficient for detecting individual nitroxides by the method introduced here — another significant simplification.

Tip material. Thermomagnetic noise in the tip can degrade both T_1 and $T_{1\rho}$ (33, 34) and, in magnet-on-cantilever experiments, can lead to a degradation of cantilever Q at high magnetic field (34, 35). Here, the Q degradation was completely mitigated by orienting the field along the width of the cantilever (13, 29) [at the expense of a twofold reduction in G' , compared with an experiment in which the tip magnetization points toward the sample plane (10)]. Thermomagnetic tip fluctuations can be suppressed

by using a high-coercivity magnetic material for the tip (like SmCo) and operating at low field (34) or by using a low-coercivity material (like Ni) and operating at high field (35). The single-electron spin experiment of ref. 10 used a SmCo tip, which had to be affixed by hand to the cantilever and whose diameter was limited to approximately 150 nm by ion-beam-milling damage. Our detection approach operates well at high field, opening up the exciting possibility of using a nickel tip, which is significantly easier to deposit and lithographically pattern to sub-100 nm dimensions.

Conclusion

The approach presented here dramatically expands the range of samples suitable for characterization by mechanically detected magnetic resonance by using ultrasensitive cantilevers and opens up a new route to achieving single-electron sensitivity in reasonable averaging times. As with cryoelectron microscopy, extending our studies from a model system to a biomacromolecule will demand a significant investment in developing sample preparation protocols. Detailed studies of the mechanisms of cantilever frequency surface noise over such samples will be required to establish the ultimate limits of the approach to single-spin detection outlined above. Nevertheless, our findings clearly establish individual spin-labeled biomacromolecules as exciting possible targets for a single electron-spin experiment and suggest that research into preparing biological samples for cryogenic magnetic resonance force microscopy should be aggressively pursued.

ACKNOWLEDGMENTS. We acknowledge Doran Smith and the U.S. Army Research Laboratory (Adelphi, MD) for their generous loan of the microwave source and amplifier used here. We acknowledge Brian Crane and Barbara Baird for helpful discussions on spin-labeling biomacromolecules. This work was supported by National Institutes of Health Grant 5R01GM-070012 (to J. A. M.), National Center for Research Resources Center Grant P41RR016292 (to J. H. F.), and the Army Research Office Multi-University Research Initiative Grant W911NF-05-1-0403 (to J. A. M.). This work was performed in part at the Cornell NanoScale Science and Technology Facility, a member of the National Nanotechnology Infrastructure Network, which is supported by National Science Foundation Grant ECS-0335765.

- Altenbach C, Marti T, Khorana HG, Hubbell WL (1990) Transmembrane protein structure—Spin labeling of bacteriophodopsin mutants. *Science* 248:1088–1092.
- Hubbell WL, Gross A, Langen R, Lietzow MA (1998) Recent advances in site-directed spin labeling of proteins. *Curr Opin Struct Biol* 8:649–656.
- Borbat PP, Costa-Filho AJ, Earle KA, Moscicki JK, Freed JH (2001) Electron spin resonance in studies of membranes and proteins. *Science* 291:266–269.
- Schiemann O, et al. (2004) A PELDOR-based nanometer distance ruler for oligonucleotides. *J Am Chem Soc* 126:5722–5729.
- Borbat PP, Davis JH, Butcher SE, Freed JH (2004) Measurement of large distances in biomolecules using double-quantum filtered refocused electron spin-echoes. *J Am Chem Soc* 126:7746–7747.
- Malmberg NJ, Falke JJ (2005) Use of EPR power saturation to analyze the membrane-docking geometries of peripheral proteins: Applications to C2 domains. *Ann Rev Biophys Biomol Struct* 34:71–90.
- Park SY, et al. (2006) Reconstruction of the chemotaxis receptor-kinase assembly. *Nat Struct Mol Biol* 13:400–407.
- Cai Q, et al. (2006) Site-directed spin labeling measurements of nanometer distances in nucleic acids using a sequence-independent nitroxide probe. *Nucleic Acids Res* 34:4722–4730.
- Blank A, Freed JH (2006) ESR microscopy and nanoscopy with “induction” detection. *Isr J Chem* 46:423–438.
- Rugar D, Budakian R, Mamin HJ, Chui BW (2004) Single spin detection by magnetic resonance force microscopy. *Nature* 430:329–332.
- Rugar D, et al. (1994) Force detection of nuclear magnetic resonance. *Science* 264:1560–1563.
- Sidles JA, et al. (1995) Magnetic resonance force microscopy. *Rev Mod Phys* 67:249–265.
- Garner SR, Kuehn S, Dawlaty JM, Jenkins NE, Marohn JA (2004) Force-gradient detected nuclear magnetic resonance. *Appl Phys Lett* 84:5091–5093.
- Kuehn S, Hickman SA, Marohn JA (2008) Advances in mechanical detection of magnetic resonance. *J Chem Phys* 128:052208.
- Degen CL, Poggio M, Mamin HJ, Rettner CT, Rugar D (2009) Nanoscale magnetic resonance imaging. *Proc Natl Acad Sci USA* 106:1313–1317.
- Du JL, Eaton GR, Eaton SS (1995) Temperature, orientation, and solvent dependence of electron spin-lattice relaxation rates for nitroxyl radicals in glassy solvents and doped solids. *J Magn Reson A* 115:213–221.
- Zhou Y, Bowler BE, Eaton GR, Eaton SS (1999) Electron spin lattice relaxation rates for $S = 1/2$ molecular species in glassy matrices or magnetically dilute solids at temperatures between 10 and 300 K. *J Magn Reson* 139:165–174.
- Farrar CT, Hall DA, Gerfen GJ, Inati SJ, Griffin RG (2001) Mechanism of dynamic nuclear polarization in high magnetic fields. *J Chem Phys* 114:4922–4933.
- Mamin H, Budakian R, Chui B, Rugar D (2003) Detection and manipulation of statistical polarization in small spin ensembles. *Phys Rev Lett* 91:207604.
- Rugar D, Yannoni CS, Sidles JA (1992) Mechanical detection of magnetic resonance. *Nature* 360:563–566.
- Lee SG, Won S, Saun Sb, Lee S (2007) Magnetic resonance force microscopy in fast-relaxing spins using a frequency-modulation mode detection method. *Nanotechnology* 18:375505.
- Mamin HJ, Poggio M, Degen CL, Rugar D (2007) Nuclear magnetic resonance imaging with 90-nm resolution. *Nature Nanotech* 2:301–306.
- Stowe TD, et al. (1997) Attonewton force detection using ultrathin silicon cantilevers. *Appl Phys Lett* 71:288–290.
- Jenkins NE, et al. (2004) Batch fabrication and characterization of ultrasensitive cantilevers with submicron magnetic tips. *J Vac Sci Technol B* 22:909–915.
- Stipe BC, Mamin HJ, Stowe TD, Kenny TW, Rugar D (2001) Noncontact friction and force fluctuations between closely spaced bodies. *Phys Rev Lett* 87:09:6801.
- Kuehn S, Loring RF, Marohn JA (2006) Dielectric fluctuations and the origins of noncontact friction. *Phys Rev Lett* 96:156103.
- Kuehn S, Marohn JA, Loring RF (2006) Noncontact dielectric friction. *J Phys Chem B* 110:14525–14528.
- Yazdani SM, Marohn JA, Loring RF (2008) Dielectric fluctuations in force microscopy: Noncontact friction and frequency jitter. *J Chem Phys* 128:224706.
- Marohn JA, Fainchtein R, Smith DD (1998) An optimal magnetic tip configuration for magnetic-resonance force microscopy of microscale buried features. *Appl Phys Lett* 73:3778–3780.
- Wago K, Botkin D, Yannoni CS, Rugar D (1998) Paramagnetic and ferromagnetic resonance imaging with a tip-on-cantilever magnetic resonance force microscope. *Appl Phys Lett* 72:2757–2759.
- Albrecht TR, Grütter P, Horne D, Rugar D (1991) Frequency-modulation detection using high-Q cantilevers for enhanced force microscope sensitivity. *J Appl Phys* 69:668–673.
- Dougherty W, et al. (2000) The Bloch equations in high-gradient magnetic resonance force microscopy: Theory and experiments. *J Magn Reson* 143:106–119.
- Hannay JD, Chantrell RW, Rugar D (2000) Thermal field fluctuations in a magnetic tip/implications for magnetic resonance force microscopy. *J Appl Phys* 87:6827–6829.
- Stipe BC, et al. (2001) Electron spin relaxation near a micron-size ferromagnet. *Phys Rev Lett* 87:277602.
- Ng TN, Jenkins NE, Marohn JA (2006) Thermomagnetic fluctuations and hysteresis loops of magnetic cantilevers for magnetic resonance force microscopy. *IEEE Trans Mag* 42:378.
- Bruland K, Dougherty W, Garbini J, Sidles J, Chao S (1998) Force-detected magnetic resonance in a field gradient of 250 000 tesla per meter. *Appl Phys Lett* 73:3159–3161.
- Mozyrsky D, Martin I, Pelekchov D, Hammel P (2003) Theory of spin relaxation in magnetic resonance force microscopy. *Appl Phys Lett* 82:1278–1280.
- Mamin H, Budakian R, Rugar D (2003) Superconducting microwave resonator for millikelvin magnetic resonance force microscopy. *Rev Sci Instrum* 74:2749–2753.